Article

The Study of HIV-1 Vpr-Membrane and Vpr-hVDAC-1 Interactions by Graphene Field-Effect Transistor Biosensors

Peibin Zhong,[#] Chun-Hao Liu,[#] Yit-Tsong Chen,* and Tsyr-Yan Yu*

Cite This: *ACS Appl. Bio Mater.* 2020, 3, 6351−6357

Read Online

ACCESS | Metrics & More | Article Recommendations | SI Supporting Information

ABSTRACT: The viral protein R (Vpr) of human immunodeficiency virus 1 (HIV-1) is involved in many cellular processes during the viral life cycle; however, its associated mechanisms remain unclear. Here, we designed an *Escherichia coli* expression construct to achieve a milligram yield of recombinant Vpr. In addition, we fabricated a graphene field-effect transistor (G-FET) biosensor, with the modification of a supported lipid bilayer (SLB), to study the interaction between Vpr and its interaction partners. The Dirac point of the SLB/G-FET was observed to shift in response to the binding of Vpr to the SLB. By fitting the normalized shift of the Dirac point as a function of Vpr concentration to the Langmuir adsorption isotherm equation, we could extract the dissociation constant (K_d) to quantify the Vpr binding affinity. When the 1,2-dioleoyl-*sn*-glycero-3-phospho-(1′-rac-glycerol) (DOPG) membrane was used as the SLB, the dissociation constant was determined to be 9.6 ± 2.1 μM. In contrast, only a slight shift of the Dirac point was observed in response to the addition of Vpr when the 1,2-dioleoyl-*sn*-glycero-3-phosphocholine (DOPC) membrane was used as the SLB. Taking advantage of the much weaker binding of Vpr to the DOPC membrane, we prepared a human voltage-dependent anion channel isoform 1 (hVDAC-1)-embedded DOPC membrane as the SLB for the G-FET and used it to determine the dissociation constant to be 5.1 ± 0.9 μM. In summary, using the clinically relevant Vpr protein as an example, we demonstrated that an SLB/G-FET biosensor is a suitable tool for studying the interaction between a membrane-associated protein and its interaction partners.

KEYWORDS: Vpr, G-FET, VDAC, HIV-1, membrane protein, lipid composition
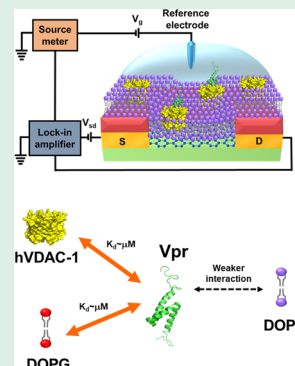
■ INTRODUCTION

The viral protein R (Vpr), expressed in the late life cycle of HIV-1, is considered an accessory viral protein.[1] Over the last three decades, a series of studies on HIV-related proteins revealed the importance of Vpr.[2−8] Vpr has been shown to play a crucial role in HIV-1 pathogenicity since the deletion of the *vpr* gene resulted in the reduction of HIV-1 virulence.[3] Vpr can induce G2/M cell cycle arrest,[4] regulate the nuclear import of the HIV-1 pre-integration complex (PIC), and enhance macrophage infection.[5−8] Additionally, Vpr can interact with the lipid membrane and form cation-selective channels in planar lipid bilayers,[9] while Vpr-containing vesicles can fuse into mitochondria and interact with the mitochondrial permeability transition pore complex and subsequently induce apoptosis.[1,2] Even though Vpr is involved in so many cellular processes, its associated mechanisms are poorly understood due to the challenges associated with protein production and biophysical characterizations. In regard to protein production, Vpr has been shown to be cytotoxic, inhibits prokaryotic cell growth, and causes plasmid instability during expression in *Escherichia coli*.[10]

Moreover, difficulties in Vpr expression were reported previously.[11] To tackle this problem, we designed an *E. coli* expression construct, in which the His-tagged GB1 domain of streptococcal protein G (GB1) was fused to the N-terminal of the Vpr protein.[12] The high production yield of several milligrams per liter of GB1-fused Vpr proteins could be obtained using both Luria−Bertani (LB) broth and a defined growth medium.

Among the various interaction partners, it has been challenging to study the interaction between Vpr and membrane-related interaction partners, and controversial results have been reported in the literature. For instance, different conclusions have been reported regarding Vpr-hVDAC-1 interactions. While no specific interaction between N-terminally biotinylated Vpr52-96 and the recombinant VDAC of *Neurospora crassa* was reported in a study using surface plasma resonance, it was reported that the gelsolin G5 domain can inhibit the interaction between Vpr and hVDAC-1.[13,14] Here, we aimed to answer if lipid composition plays a role in Vpr-membrane interaction and determine if Vpr interacts with hVDAC-1. Using a calcein release assay, we showed that GB1-fused Vpr-induced membrane permeability

was lipid composition-dependent. The calcein release rate was observed to increase as the content of DOPG was increased.

Advancements in nanotechnology in recent years led to the emergence of novel, sensitive nanoscale sensors. The high surface-to-volume ratio and the unique quantum confinements of nanomaterials make them ideal for the fabrication of biological sensors,[15] such as a graphene-based field-effect transistor (G-FET),[16−19] to probe a trace amount of target molecules in real time with label-free, sensitive, and selective detections. The binding of biomolecules on a G-FET leads to a significant potential change on the G-FET surface, resulting in the variation of conductance inside the G-FET due to an electrical gating effect. By modifying a suitable receptor on the G-FET surface, this G-FET platform can be an excellent biosensor for detecting specific target biomolecules. Moreover, because of the planar graphene surface, a G-FET is suitable for membrane-related experiments.

In this study, we designed a G-FET biosensor to quantify the interaction between Vpr and lipid membranes as illustrated in Figure 1. The binding of Vpr on the supported lipid bilayer
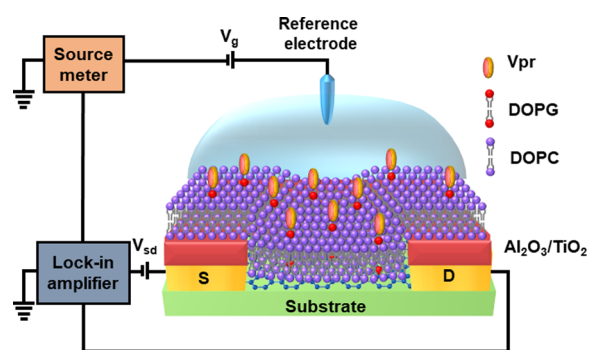

Figure 1. Schematic illustration representing the application of a G-FET for measuring lipid-membrane interactions. The SLB is paved on top of the graphene channel to form an SLB/G-FET biosensor. While Vpr interacts with the SLB, the surface potential of the SLB/G-FET changes and subsequently modulates the channel current of the G-FET, the signal of which is collected by a lock-in amplifier. While the source-drain voltage (V_{sd}) is applied from the lock-in amplifier, a Ag/AgCl electrode is used as a solution gate with the voltage (V_g) supplied by a source meter.

membrane (SLB) on a G-FET would result in a shift of the transfer curve of the biosensor. Using a G-FET biosensor, we measured the interaction between Vpr and lipid membranes consisting of 1,2-dioleoyl-sn-glycero-3-phospho-(1′-rac-glycerol) (DOPG) and 1,2-dioleoyl-sn-glycero-3-phosphocholine (DOPC) in a 1:1 ratio, and the dissociation constant was determined to be 9.6 ± 2.1 μM. In contrast, the interaction between Vpr and the DOPC only membrane was much weaker. We further prepared hVDAC-1 embedded in the DOPC membrane as an SLB to study the interaction between Vpr and hVDAC-1. The Dirac point shift due to the addition of Vpr was attributed to the interaction between Vpr and hVDAC-1 since only an insignificant shift in the Dirac point was observed when the DOPC only membrane was used as an SLB. The dissociation constant of Vpr interacting with hVDAC-1 was quantified by G-FET biosensors to be 5.1 ± 0.9 μM. In summary, Vpr-hVDAC-1 interaction and the lipid composition-dependent Vpr-membrane interaction were quantified by the G-FET biosensor designed in this work. We believe that the G-FET biosensor is ideal for studying the

interaction between a membrane-associated protein and its interaction partners and will be an important tool available to biologists.

MATERIALS AND METHODS

Preparation of Vpr and hVDAC-1. A detailed description of the expression construct of HIV-1 Vpr, protein production, purification, and characterization is provided in the Supporting Information. Briefly, we designed an E. coli expression construct, containing a 6x histidine tag followed by a GB1 tag and a cleavage site of the tobacco etch virus (TEV) protease, at the N-terminal. The final expression vector carried 6xHis-GB1-TEV-Vpr, hereinafter referred to as GB1-fused Vpr, as illustrated in Figure 2A. GB1, the B1 domain of
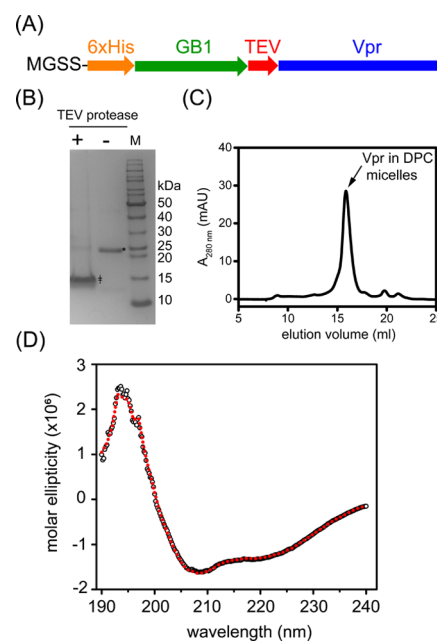
Figure 2. Expression and characterization of the Vpr protein. (A) Schematic drawing of the design of the Vpr expression plasmid. (B) SDS-PAGE analysis of GB1-fused Vpr with (+) and without (−) treatment with the TEV protease (*fused protein; ‡Vpr protein). (C) SEC elution profile and (D) experimental (open circles) and fitted (dashed line) circular dichroism (CD) spectra of Vpr solubilized in DPC micelles. The secondary structure content was analyzed by DichroWeb using the CDSSTR program and SP175 as a reference set, which was optimized for 190−240 nm.

streptococcal protein G (GB1), is generally used as a solubility enhancement partner. Protein expression under low temperature (18 °C) conditions achieved milligram yields of Vpr in LB broth and in a defined growth medium (Table S1). The E. coli-expressed GB1-fused Vpr could be purified using standard affinity chromatography and size-exclusion chromatography. For the production, purification, and preparation of human voltage-dependent anion channel isoform 1 (hVDAC-1) refolded in N,N-dimethyldodecylamine-N-oxide (LDAO) detergent micelles, we followed well-established protocols in the literature.[20,21]

Preparation of Liposomes. Four kinds of calcein-encapsulated liposomes were prepared for the calcein release assay, including liposomes made of DOPC, DOPC/DOPG (95:5, weight ratio), DOPC/DOPG (50:50, weight ratio), and DOPG. The weight ratios were used for the mixed lipids. Lipids were first dissolved in an ethanol/chloroform mixture (1:1) and then dried on the glass wall by nitrogen gas followed with a vacuum treatment for 1 h to remove the residual organic solvent. The dried lipid film was resuspended in a buffer containing 25 mM Tris at pH 7.5, 50 mM calcein, 25 mM NaCl, 0.5 mM EDTA, and 1 mM tris(2-carboxyethyl)phosphine

hydrochloride (TCEP) and homogenized by water bath sonication for 1 h followed with five freeze−thaw cycles using liquid nitrogen at 70 °C. The calcein-encapsulated liposomes were formed and homogenized using an extruder with a polycarbonate membrane with a defined pore size of 0.1 μm in diameter. The non-encapsulated calcein was removed from the liposome suspension by standard gel filtration. The calcein-containing liposomes were examined by dynamic light scattering for quality control prior to fluorescence measurement (DelsaNano C particle size and zeta potential analyzer, Beckman Coulter).

To prepare the supported lipid bilayers for G-FET sensors, four different kinds of liposomes were produced by removing the detergent molecules from the lipid-detergent or proteolipid-detergent micelle solutions. For DOPC-detergent micelle solution and DOPG-detergent micelle solution, individual lipids, either DOPC or DOPG, were first dissolved in a 50 mM solution of detergent micelles containing 25 mM Tris at pH 7.5, 200 mM Triton X-100, 100 mM NaCl, 0.5 mM EDTA, and 1 mM TCEP, respectively. Then, the lipid-detergent micelle solution was diluted to a final lipid concentration of 1 mg/mL using a Tris buffer (containing 25 mM Tris at pH 7.5, 100 mM NaCl, 0.5 mM EDTA, and 1 mM TCEP). For the DOPC/DOPG (1:1, molar ratio) lipid-detergent micelle solution, the abovementioned DOPG and DOPC lipid-detergent micelle solutions were mixed at a 1:1 ratio and diluted to 1 mg/mL of the total lipid concentration using the Tris buffer mentioned above. For hVDAC-1 proteolipid-detergent micelles, a 50 mM DOPC lipid was first dissolved in a sodium phosphate buffer (containing 25 mM sodium phosphate at pH 6.5, 200 mM sodium cholate, 100 mM NaCl, 0.5 mM EDTA, 5 mM TCEP, and 0.1% LDAO). Subsequently, the DOPC lipid was diluted to 1 mg/mL in the LDAO-solubilized hVDAC-1 solution (25 mM sodium phosphate at pH 6.5, 0.3 mg/mL hVDAC-1, 100 mM NaCl, 0.5 mM EDTA, 5 mM TCEP, 1× cOmplete protease inhibitor cocktail, and 0.1% LDAO). The molar ratio of hVDAC-1 to DOPC was 1:136. To initiate the formation of liposomes or proteoliposomes, Bio-Beads SM-2 (BioRad, Hercules, CA) were added to each lipid-detergent at a density of 90 mg per 1 mL or proteolipid-detergent micelle solution, at a density of 80 mg per 100 μL, and gently shaken at 4 °C for 12 h. This was followed by filtering centrifugation to remove biobeads, and the liposomes and proteoliposomes were homogenized using an extruder with a polycarbonate membrane with a defined pore size of 0.05 μm in diameter.

Calcein Release Assay. The permeabilization of liposomes by GB1-fused Vpr can be studied by monitoring the release of the encapsulated calcein. Calcein is a membrane-impermeable fluorescent probe. When encapsulated, calcein undergoes self-quenching at high concentration. The fluorescence signal was expected to increase as the calcein molecules were released from the liposome due to Vpr binding, which destabilized the membrane bilayer. A luminescence spectrometer (PerkinElmer LS55) was used to record the fluorescence emission spectra, ranging from 505 to 535 nm, with the excitation wavelength at 495 nm. We recorded the fluorescence spectra immediately after the addition of GB1-fused Vpr for 25 min with 30 s intervals. The peak intensity of the calcein fluorescence spectrum was observed to be at 517 nm. The negative control experiments were performed by mixing the liposome with a buffer containing 25 mM Tris at pH 7.5, 25 mM NaCl, 0.5 mM EDTA, and 1 mM TCEP, while the positive control experiments were performed with a buffer containing 25 mM Tris at pH 7.5, 0.3% Triton X-100, 25 mM NaCl, 0.5 mM EDTA, and 1 mM TCEP. For each experimental condition, three replicates of experiments were performed. The time course of the calcein release was quantified according to the equation calcein release$(t) = (I_{\text{Vpr}(t)} - I_{\text{buffer}(t)})/(I_{\text{TX}-100} - I_{\text{buffer}(t)})$, where $I_{\text{Vpr}(t)}$ is the intensity of the fluorescence signal at 517 nm for the samples with the addition of the GB1-fused Vpr protein, and $I_{\text{TX}-100}$ and $I_{\text{buffer}(t)}$ are the intensities for the positive and the negative controls, respectively.

Device Fabrication of G-FETs. A set of 4 in. Si wafers (thermal oxide, 3000 Å; thickness, 525 ± 25 μm; p-boron) was purchased from Summit-Tech and diced into pieces of 16 × 16 mm^2 in size. The diced Si wafers were rinsed sequentially with acetone, isopropanol, and deionized water for 10 min followed by a N$_2$ blow and an O$_2$ plasma treatment (100 W; O$_2$, 50 sccm) for 3.3 min.

A monolayer CVD-grown graphene film (2.5 × 2.5 cm^2) on a polymer substrate was purchased from ACS Material. A proper size (~2 × 2 mm^2) of the graphene film was cut and transferred onto a Si wafer (16 × 16 mm^2) with the assistance of poly(methylmethacrylate) (PMMA). In the transfer process, a suspended PMMA/graphene film was rinsed in deionized water, transferred onto the Si wafer, and dried in ambient air for 30 min followed by baking at 100 °C for 20 min. PMMA was dissolved in acetone at 50 °C for 30 min (Figure S1a). The graphene film, used as a conducting channel (with a length of 2 μm and a width of 1 μm) of a FET device, was patterned by photolithography and casted by O$_2$ plasma (18 W; O$_2$, 50 sccm) for 2.5 min (Figure S1b). A pair of source and drain electrodes (Cr/Au = 5/50 nm in thickness) was patterned by photolithography and subsequently deposited on both ends of the graphene channel with a thermal evaporation method, where the deposition rates of Cr and Au were 0.5 and 1.0 Å/s, respectively. The Cr/Au electrodes were then coated with Al$_2$O$_3$/TiO$_2$ (60/5 nm in thickness) insulating layers sequentially by atomic-layer deposition to avoid electrical leakage in the following biosensing measurements. The liftoff of photoresistors on the as-fabricated devices was facilitated with a sonicator (Figure S1c).

Preparation of SLB/G-FETs. In preparing an SLB/G-FET biosensor, a polydimethylsiloxane (PDMS) reservoir was built on the Si wafer containing the as-fabricated G-FET device to accommodate sample solutions. PDMS, a blend of Sylgard 184A/184B = 10:1 solution, was evacuated to remove bubbles and cured by baking at 80 °C for 15 min. To pave the SLB on a G-FET, 100 μL of a liposome suspension was dropped into the PDMS reservoir and kept at ambient conditions for 1 h. The lipid bilayers were assembled onto graphene via vesicle fusion (Figure S1d).[22] Subsequently, the unbounded liposomes were removed, and the reservoir was washed extensively with a Tris buffer solution containing 25 mM Tris at pH 6.0, 25 mM NaCl, and 0.5 mM EDTA.

Electrical Measurements. The transfer curves (i.e., the source-drain current (I_{sd}) vs. solution-gate (V_{g}) plots) of SLB/G-FETs were measured with a lock-in amplifier (Stanford Research System, SR830) conducted at a bias voltage (V_{sd}) of 8 mV, a modulation frequency of 113 Hz, and a time constant of 100 ms. The electrical measurements using an SLB/G-FET biosensor can also be found in our previous publication.[19] For the detection of Vpr by an SLB/G-FET, different concentrations of GB1-fused Vpr and the TEV protease were diluted separately into a Tris buffer solution (containing 25 mM Tris at pH 7.5, 25 mM NaCl, 0.5 mM EDTA, and 1 mM TCEP). To prepare for the electrical measurement, GB1-fused Vpr was added directly onto the SLB/G-FET device (Figure S1e) and incubated at 25 °C for 30 min with gentle shaking. The GB1 was then removed by the treatment of the TEV protease (Figure S1f,g) for 30 min. The SLB/G-FET device was then washed extensively using a Tris buffer solution containing 25 mM Tris at pH 6.0, 25 mM NaCl, and 0.5 mM EDTA to remove GB1. For the electrical measurements, to obtain the transfer curves of an SLB/G-FET device, a Ag/AgCl electrode was used as a solution gate with the voltage supplied by a source meter (Keithley 2400). During the biosensing measurements to detect the lipid-protein interactions, the whole SLB/G-FET system was grounded to minimize electrical noises from the environment.

■ RESULTS AND DISCUSSIONS

Recombinant Vpr Expression and Characterizations. The involvement of Vpr in HIV-1 pathogenesis makes Vpr an important viral accessory protein. However, research to unveil how Vpr is involved in the various cellular processes has been impeded by the difficulty in expressing the recombinant protein for further characterization. E. coli expression of recombinant Vpr has been challenging due to the cytotoxicity of Vpr that inhibits bacterial cell growth and destabilizes the

plasmid. To alleviate the problem, we adopted a strategy of expressing the desired protein with a fusion partner, as shown in Figure 2A. The chosen fusion partner, GB1, was shown to greatly enhance the production yield of Vpr when the *E. coli* expression was performed at 18 °C. Also, the highly soluble nature of GB1 made GB1-fused Vpr soluble, which greatly eases the subsequent protein purification. To make sure that the fused construct could be used to express efficient and cost-effective isotope-labeled Vpr, we further tested the expression of Vpr using the defined growth medium described in Table S1. The yields of both soluble and insoluble GB1-fused Vpr protein were quantified by 280 nm absorption using a NanoDrop 2000c spectrophotometer (Thermo Fisher Scientific, Waltham, MA, USA) and are listed in Table S2. The extinction coefficient was 32,430 $M^{-1} cm^{-1}$ for GB1-fused Vpr, calculated using ProtParam available through the ExPasy server.[23] Surprisingly, the production yield of the protein was found to be higher using the defined growth medium when compared to LB broth. It is outside the scope of this work to discuss why Vpr protein production favors low-temperature *E. coli* expression in the defined growth medium. However, it is important to mention that using low-temperature expression with the defined growth medium is crucial for achieving the high expression yield. As indicated in Figure 2B, sodium dodecyl sulfate-polyacrylamide gel electrophoresis (SDS-PAGE) analysis showed that the GB1 domain of the fused protein could be removed by overnight treatment with the TEV protease at 30 °C at a molar ratio of GB1-fused Vpr protein to TEV of 20:1. The Vpr protein was precipitated after the treatment with the TEV protease.

To further obtain pure Vpr proteins, the protein precipitates were dissolved in 70% acetonitrile containing 0.1% TFA and applied to HPLC using the C18 column with an acetonitrile gradient from 40 to 80% to remove the residual TEV and GB1. The HPLC-purified Vpr proteins were characterized using a liquid chromatography-electrospray ionization-mass spectrometry (LC/ESI-MS) method using an LTQ FT Ultra (Thermo Scientific) to confirm that the correct proteins were obtained (Table S3). The observed masses were consistent with the calculated monoisotopic masses, showing that the proteins were correct. The structure of the full-length Vpr protein, as well as 1-51 Vpr and 52-96 Vpr, have been previously determined in the presence of 30% 2,2,2-trifluoroethanol (TFE), mainly due to the poor solubility of the Vpr protein.[24] Also, the structure information of the full-length Vpr was obtained in water at acidic pH in the presence of acetonitrile. These studies contributed to our current understanding of the structure of Vpr, which exhibits three α-helix segments. Instead of preparing Vpr in extreme conditions, we examined whether full-length Vpr could be solubilized in DPC detergent micelles. Early cellular-based studies showed evidence of Vpr-induced cell membrane permeabilization and death. In addition, the involvement of Vpr in apoptosis was shown to be via interacting with the mitochondrial permeability transition pore complex. Thus, the study of Vpr in the membrane-mimicking environment may provide insights into its interaction with the membrane. Previously, the structure of Vpr peptide 34-51 solubilized in DPC detergent micelles was studied with NMR spectroscopy.[24,25] It was found to contain an amphipathic, leucine zipper-like α-helix.

Here, we successfully solubilized Vpr in DPC detergent micelles. The DPC-solubilized Vpr was around 40 kDa, estimated using the elution profile of size-exclusion chroma-

tography shown in Figure 2C. The secondary structure analysis of CD spectra suggested that Vpr in DPC detergent micelles exhibits a significant fraction of α-helix features as shown in Figure 2D. The content of the α-helix did not change significantly when Vpr was transferred to bicelles from DPC micelles (Figure S2 and Table S4).

Calcein Release Assay. To further study the interaction between Vpr and membranes, we applied a calcein release assay to examine Vpr-induced release of the encapsulated calcein from liposomes. As shown in Figure 3, we observed
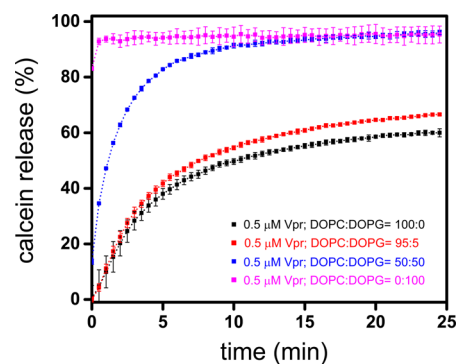

Figure 3. Lipid composition-dependent permeabilization of liposomes by GB1-fused Vpr at a concentration of 0.5 μM. Kinetics of calcein leakage of liposomes of various lipid compositions (DOPC/DOPG). The extent of calcein release was quantified relative to a positive control (100%) sample that was solubilized with Triton X-100 detergent micelles and a negative control (0%) sample with only buffer. The values are averages of triplicate assays in three experiments, with error bars representing standard deviation.

lipid composition-dependent permeabilization of liposomes by GB1-fused Vpr. As the content of DOPG increased, we observed faster release of calcein from liposomes, suggesting that the interaction between GB1-fused Vpr and membranes is lipid composition-dependent. This lipid composition-dependent Vpr-membrane interaction was also observed using lipid nanodisc coassembly assays. We assembled lipid nanodiscs in the presence of GB1-fused Vpr and then applied the TEV protease to remove GB1.

Finally, size-exclusion chromatography (SEC) was used to obtain nanodisc fractions. As shown in the SDS-PAGE analysis, Figure S3, Vpr was found to be incorporated into lipid nanodiscs assembled in the presence of DOPG, while no detectable amount of Vpr was found to be embedded in nanodiscs assembled with DOPC only. Apart from the lipid composition-dependent Vpr-membrane interaction, we also observed that GB1-fused Vpr promoted a concentration-dependent leakage of liposomes, as indicated in Figure S4. This result is consistent with the previous finding of the membrane interaction with the C-terminal peptide of Vpr.[26]

Quantification of Vpr-Membrane Interaction Using an SLB/G-FET Biosensor. An SLB/G-FET biosensor was used to evaluate the Vpr-membrane interactions. In the electrical measurements with SLB/G-FETs, the leakage current (measured from the solution gate to the drain electrode as illustrated in Figure 1) was typically less than ∼5% of the channel current (i.e., the source-drain current through the graphene channel in Figure 1), indicating good device quality. In addition, essential quality checks were performed to show that neither bare graphene, nor the lipid membrane, interacted with the TEV protease, which was used to remove the GB1 tag
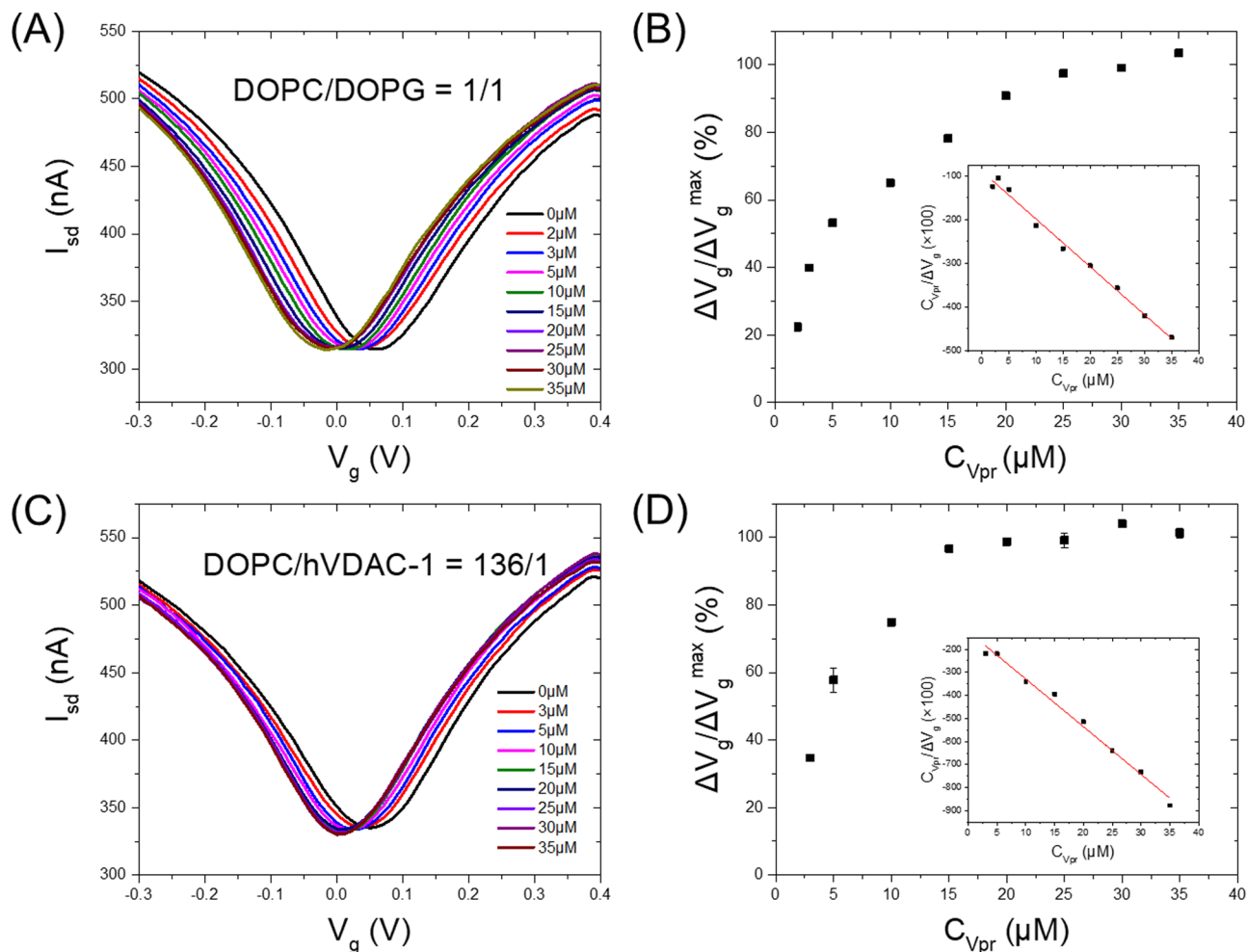
Figure 4. Transfer curves of an SLB/G-FET biosensor as a function of C_{Vpr}. (A) Transfer curves of an SLB/G-FET biosensor, where the SLB contained a mixture of DOPC/DOPG at a 1:1 ratio, recorded as a function of C_{Vpr} from 0 to 35 μM. (B) $\Delta V_g/\Delta V_g^{max}$ vs. C_{Vpr} plot summarized from the data points measured in A, where ΔV_g is the shift of the Dirac point relative to the buffer solution (without Vpr), and ΔV_g^{max} represents the saturated ΔV_g at high C_{Vpr}. The inset shows a least-squares fit of the measured data points to the Langmuir adsorption isotherm model, from which the dissociation constant of $K_d = 9.6 \pm 2.1$ μM for the Vpr-DOPC/DOPG complex was determined. (C) Transfer curves of an SLB/G-FET biosensor recorded as a function of C_{Vpr} from 0 to 35 μM, where the SLB was prepared with a mixture of DOPC/hVDAC-1 = 136:1. (D) Normalized ΔV_g plotted as a function of C_{Vpr} with the data points taken from C. In the inset, a least-squares fit of the measured data points to the Langmuir adsorption isotherm model gives $K_d = 5.1 \pm 0.9$ μM for the Vpr-hVDAC-1/DOPC complex. The standard deviation was calculated from three individual measurements.

from the GB1-fused Vpr (Figure S5). The transfer curves of an SLB/G-FET biosensor in response to various concentrations of Vpr (C_{Vpr}) were recorded to analyze the binding of Vpr to the SLB, where diverse SLBs prepared with different lipid compositions were also tested. As shown in Figure 4A, we clearly observed the shift of the transfer curve of the SLB/G-FET in response to an increasing C_{Vpr} when 50% DOPG was incorporated in the preparation of the SLB. The left shifts of the Dirac point of the G-FET due to the additions of Vpr indicated the interaction of positively charged Vpr with the DOPC/DOPG membrane to induce n-doping in the G-FET. Measuring the shift of the Dirac point in the transfer curve (Figure 4A), we plotted the normalized $\Delta V_g/\Delta V_g^{max}$ as a function of C_{Vpr}, where ΔV_g is the shift of the Dirac point relative to the reference point at $C_{Vpr} = 0$ M (before adding Vpr), and ΔV_g^{max} represents the saturated ΔV_g at high C_{Vpr}. To quantify the binding of Vpr to the SLB of DOPC/DOPG (1:1), we performed a least-squares fit of the measured data points to the Langmuir adsorption isotherm model,[19,27] from

which a dissociation constant of $K_d = 9.6 \pm 2.1$ μM for the Vpr-DOPC/DOPG complex was determined. As indicated in Figure S6, the membrane binding affinity of Vpr did not change significantly when the DOPG content was increased from 50 to 100%. In contrast, only a slight shift of the transfer curve of the SLB/G-FET was observed in response to various C_{Vpr} at 0−35 μM (as plotted in Figure S7) when the SLB was prepared with 100% DOPC lipids. This result suggests that the interaction between Vpr and the DOPC membrane is much weaker compared to the interaction between Vpr and the DOPG-containing membrane. This result is consistent with the observation from the calcein release assay, which showed that the rate of Vpr-induced permeabilization was increased as the DOPG content increased.

Together with results obtained from the calcein release assay, Vpr, resembling some cationic antimicrobial peptides, was shown to have strong interactions with anionic lipid DOPG, while it weakly interacted with the zwitterionic lipid DOPC.[28−32] Even though surface plasmon resonance technol-

ogy is used intensively to study the protein-membrane interactions,[33] it is worth mentioning that the popular L1 chip[34] cannot be applied to the current study due to the existence of a non-specific interaction between Vpr and the chip.

Quantification of Vpr-hVDAC-1 Interaction. It has been shown via cellular-based assays and pull-down assays that Vpr can interact with hVDAC-1, an important part of the mitochondrial permeability transition pore complex.[13,14] When studying the interaction between Vpr and hVDAC-1 embedded in the membrane, it is difficult to decouple Vpr-membrane interaction from Vpr-membrane protein interaction. To tackle this problem, we chose to use hVDAC-1 embedded in the DOPC membrane as the SLB for an SLB/G-FET biosensor since the interaction between Vpr and the DOPC membrane is not significant as described in the previous section. We further confirmed that there is no interaction between Vpr and bare graphene, as shown in Figure S7. The detected shifts of the transfer curves of an SLB/G-FET biosensor in response to the titration of Vpr, as shown in Figure 4C, were resulted from Vpr binding to hVDAC-1 since Vpr does not interact with the DOPC membrane nor graphene. It is clearly observed from Figure 4C that the shift of the transfer curve of the SLB/G-FET, induced by the binding of Vpr, reached a plateau value as the concentration of Vpr was increased to 35 μM (Figure 4D). To calculate the binding affinity of Vpr against hVDAC-1, we plotted the $\Delta V_g / \Delta V_g^{max}$ vs. C_{Vpr} curve (Figure 4D), where $K_d = 5.1 \pm 0.9$ μM for the Vpr-hVDAC-1 complex was determined by a least-squares fit to the Langmuir adsorption isotherm model. In physiological conditions, hVDAC-1 is embedded in the outer membrane of mitochondria, which is composed of both negatively charged lipids and neutral lipids. Based on our results, Vpr can interact with the outer membrane of mitochondria via both negative lipids and hVDAC-1.

CONCLUSIONS

Limited tools are available for characterizing the interaction between membrane-associated proteins and their interaction partners. In this work, we designed and fabricated G-FETs modified with various SLBs to answer if the clinically relevant protein, HIV-1 Vpr, interacts with membranes selectively and with hVDAC-1 specifically. The quantitative measurement results using SLB/G-FETs were consistent with the qualitative result obtained from the calcein release assay. We showed that Vpr can bind strongly to DOPG-containing membranes with an affinity in the micromolar range and can induce membrane permeability rapidly. In contrast, the affinity of Vpr and membranes consisting of DOPC only is much weaker. Given the advantage of the weak interaction between Vpr and DOPC membranes, we prepared hVDAC-1-embedded DOPC membranes as an SLB for a G-FET and used this to quantify the interaction between Vpr and hVDAC-1, which also had an affinity in the micromolar range. By demonstrating the application of SLB/G-FETs to study this clinically relevant Vpr, we believe that SLB/G-FETs provide an alternative choice for biologists to study membrane-associated proteins.

ASSOCIATED CONTENT

Supporting Information

The Supporting Information is available free of charge at https://pubs.acs.org/doi/10.1021/acsabm.0c00783.

Expression, purification, and characterization of viral protein R; solubilization of Vpr in DPC detergent micelles; preparation of Vpr in bicelles; (Figure S1) schematic illustration of the fabrication of an SLB/G-FET device and the use of this SLB/G-FET biosensor for detecting Vpr-membrane interactions; (Figure S2) CD spectra of Vpr solubilized in different membrane-mimicking systems; (Figure S3) lipid nanodisc coassembly assay; (Figure S4) protein concentration-dependent permeabilization of liposomes by GB1-fused Vpr; (Figure S5) validation experiments for examining the potential interaction between TEV and the biosensors; (Figure S6) response of the transfer curve of an SLB/G-FET device to the addition of Vpr, where the SLB was composed of DOPG; (Figure S7) control experiments for measuring the interaction of Vpr and hVDAC-1 embedded in the DOPC membrane; (Table S1) recipe for 1 L of the growth medium; (Table S2) yields of GB1-fused Vpr proteins; (Table S3) monoisotopic mass (kDa) of the proteins; (Table S4) calculated secondary structure fractions based on CD spectra (PDF)

AUTHOR INFORMATION

Corresponding Authors

Yit-Tsong Chen − *Department of Chemistry, National Taiwan University, Taipei 10617, Taiwan; Institute of Atomic and Molecular Sciences, Academia Sinica, Taipei 10617, Taiwan;* orcid.org/0000-0002-6204-8320; Email: ytcchem@ntu.edu.tw

Tsyr-Yan Yu − *Institute of Atomic and Molecular Sciences, Academia Sinica, Taipei 10617, Taiwan;* orcid.org/0000-0001-7051-4769; Email: tyyu@pub.iams.sinica.edu.tw

Authors

Peibin Zhong − *Department of Chemistry, National Taiwan University, Taipei 10617, Taiwan*

Chun-Hao Liu − *Chemical Biology and Molecular Biophysics, Taiwan International Graduate Program, Academia Sinica, Taipei 115, Taiwan; Institute of Bioinformatics and Structural Biology, National Tsing Hua University, Hsin Chu 30013, Taiwan*

Complete contact information is available at:
https://pubs.acs.org/10.1021/acsabm.0c00783

■ ABBREVIATIONS

HIV-1, human immunodeficiency virus 1; Vpr, viral protein R; hVDAC-1, human voltage-dependent anion channel isoform 1; GB1, B1 domain of streptococcal protein G; TEV, tobacco etch virus; SLB, supportive lipid bilayer; G-FET, graphene field-effect transistor; LDAO, *N,N*-dimethyldodecylamine-*N*-oxide; DOPC, 1,2-dioleoyl-*sn*-glycero-3-phosphocholine; DOPG, 1,2-dioleoyl-*sn*-glycero-3-phospho-1′-rac-glycerol; TFE, 2,2,2-trifluoroethanol; SDS-PAGE, sodium dodecyl sulfate-polyacrylamide gel electrophoresis; TCEP, tris(2-carboxyethyl)phosphine hydrochloride; PMMA, poly-(methylmethacrylate); PIC, pre-integration complex

■ REFERENCES

(1) Romani, B.; Engelbrecht, S. Human immunodeficiency virus type 1 Vpr: functions and molecular interactions. *J. Gen. Virol.* **2009**, *90*, 1795−1805.

(2) Rice, A. P.; Kimata, J. T. Subversion of Cell Cycle Regulatory Mechanisms by HIV. *Cell Host Microbe* **2015**, *17*, 736−740.

(3) Gibbs, J. S.; Lackner, A. A.; Lang, S. M.; Simon, M. A.; Sehgal, P. K.; Daniel, M. D.; Desrosiers, R. C. Progression to Aids in the Absence of a Gene for Vpr or Vpx. *J. Virol.* **1995**, *69*, 2378−2383.

(4) He, J.; Choe, S.; Walker, R.; Di Marzio, P.; Morgan, D. O.; Landau, N. R. Human Immunodeficiency Virus Type 1 Viral-Protein R (Vpr) Arrests Cells in the G2 Phase of the Cell Cycle by Inhibiting P34Cdc2 Activity. *J. Virol.* **1995**, *69*, 6705−6711.

(5) Jenkins, Y.; McEntee, M.; Weis, K.; Greene, W. C. Characterization of HIV-1 Vpr nuclear import: Analysis of signals and pathways. *J. Cell Biol.* **1998**, *143*, 875−885.

(6) Popov, S.; Rexach, M.; Zybarth, G.; Reiling, N.; Lee, M.-A.; Ratner, L.; Lane, C. M.; Moore, M. S.; Blobel, G.; Bukrinsky, M. Viral protein R regulates nuclear import of the HIV-1 pre-integration complex. *EMBO J.* **1998**, *17*, 909−917.

(7) Kamata, M.; Nitahara-Kasahara, Y.; Miyamoto, Y.; Yoneda, Y.; Aida, Y. Importin-alpha promotes passage through the nuclear pore complex of human immunodeficiency virus type 1 Vpr. *J. Virol.* **2005**, *79*, 3557−3564.

(8) Piller, S. C.; Ewart, G. D.; Premkumar, A.; Cox, G. B.; Gage, P. W. Vpr protein of human immunodeficiency virus type 1 forms cation-selective channels in planar lipid bilayers. *Proc. Natl. Acad. Sci.* **1996**, *93*, 111−115.

(9) Mologni, D.; Citterio, P.; Menzaghi, B.; Poma, B. Z.; Riva, C.; Broggini, V.; Sinicco, A.; Milazzo, L.; Adorni, F.; Rusconi, S.; Galli, M.; Riva, A.; rHoPeS Group.. Vpr and HIV-1 disease progression: R77Q mutation is associated with long-term control of HIV-1 infection in different groups of patients. *Aids* **2006**, *20*, 567−574.

(10) Tachiwana, H.; Shimura, M.; Nakai-Murakami, C.; Tokunaga, K.; Takizawa, Y.; Sata, T.; Kurumizaka, H.; Ishizaka, Y. HIV-1 Vpr induces DNA double-strand breaks. *Cancer Res.* **2006**, *66*, 627−631.

(11) Bodéus, M.; Margottin, F.; Durand, H.; Rouer, E.; Benarous, R. Inhibition of prokaryotic cell growth by HIV1 Vpr. *Res. Virol.* **1997**, *148*, 207−213.

(12) Zhou, P.; Wagner, G. Overcoming the solubility limit with solubility-enhancement tags: successful applications in biomolecular NMR studies. *J. Biomol. NMR* **2010**, *46*, 23−31.

(13) Jacotot, E.; Ravagnan, L.; Loeffler, M.; Ferri, K. F.; Vieira, H. L. A.; Zamzami, N.; Costantini, P.; Druillennec, S.; Hoebeke, J.; Briand, J. P.; Irinopoulou, T.; Daugas, E.; Susin, S. A.; Cointe, D.; Xie, Z. H.; Reed, J. C.; Roques, B. P.; Kroemer, G. The HIV-1 viral protein R induces apoptosis via a direct effect on the mitochondrial permeability transition pore. *J. Exp. Med.* **2000**, *191*, 33−46.

(14) Qiao, H.; McMillan, J. R. Gelsolin segment 5 inhibits HIV-induced T-cell apoptosis via Vpr-binding to VDAC. *FEBS Lett.* **2007**, *581*, 535−540.

(15) Chen, K.-I.; Li, B.-R.; Chen, Y.-T. Silicon Nanowire Field-Effect Transistor-Based Biosensors for Biomedical Diagnosis and Cellular Recording Investigation. *Nano Today* **2011**, *6*, 131−154.

(16) Ang, P. K.; Chen, W.; Wee, A. T. S.; Loh, K. P. Solution-Gated Epitaxial Graphene as pH Sensor. *J. Am. Chem. Soc.* **2008**, *130*, 14392−14393.

(17) Ono, T.; Kanai, Y.; Inoue, K.; Watanabe, Y.; Nakakita, S.-i.; Kawahara, T.; Suzuki, Y.; Matsumoto, K. Electrical Biosensing at Physiological Ionic Strength Using Graphene Field-Effect Transistor in Femtoliter Microdroplet. *Nano Lett.* **2019**, *19*, 4004−4009.

(18) Hu, S.-K.; Lo, F.-Y.; Hsieh, C.-C.; Chao, L. Sensing Ability and Formation Criterion of Fluid Supported Lipid Bilayer Coated Graphene Field-Effect Transistors. *ACS Sens.* **2019**, *4*, 892−899.

(19) Kuo, C.-J.; Chiang, H.-C.; Tseng, C.-A.; Chang, C.-F.; Ulaganathan, R. K.; Ling, T.-T.; Chang, Y.-J.; Chen, C.-C.; Chen, Y.-R.; Chen, Y.-T. Lipid-modified graphene-transistor biosensor for monitoring amyloid-β aggregation. *ACS Appl. Mater. Interfaces* **2018**, *10*, 12311−12316.

(20) Hiller, S.; Garces, R. G.; Malia, T. J.; Orekhov, V. Y.; Colombini, M.; Wagner, G. Solution structure of the integral human membrane protein VDAC-1 in detergent micelles. *Science* **2008**, *321*, 1206−1210.

(21) Raschle, T.; Hiller, S.; Yu, T. Y.; Rice, A. J.; Walz, T.; Wagner, G. Structural and Functional Characterization of the Integral Membrane Protein VDAC-1 in Lipid Bilayer Nanodiscs. *J. Am. Chem. Soc.* **2009**, *131*, 17777−17779.

(22) Castellana, E. T.; Cremer, P. S. Solid supported lipid bilayers: From biophysical studies to sensor design. *Surf. Sci. Rep.* **2006**, *61*, 429−444.

(23) Gasteiger, E.; Gattiker, A.; Hoogland, C.; Ivanyi, I.; Appel, R. D.; Bairoch, A. ExPASy: the proteomics server for in-depth protein knowledge and analysis. *Nucleic Acids Res.* **2003**, *31*, 3784−3788.

(24) Wecker, K.; Morellet, N.; Bouaziz, S.; Roques, B. P. NMR structure of the HIV-1 regulatory protein Vpr in H2O/trifluoroethanol. Comparison with the Vpr N-terminal (1-51) and C-terminal (52-96) domains. *Eur. J. Biochem.* **2002**, *269*, 3779−3788.

(25) Engler, A.; Stangler, T.; Willbold, D. Structure of human immunodeficiency virus type 1 Vpr(34-51) peptide in micelle containing aqueous solution. *Eur. J. Biochem.* **2002**, *269*, 3264−3269.

(26) Coeytaux, E.; Coulaud, D.; Le Cam, E.; Danos, O.; Kichler, A. The cationic amphipathic alpha-helix of HIV-1 viral protein R (Vpr) binds to nucleic acids, permeabilizes membranes, and efficiently transfects cells. *J. Biol. Chem.* **2003**, *278*, 18110−18116.

(27) Anand, A.; Liu, C.-R.; Chou, A.-C.; Hsu, W.-H.; Ulaganathan, R. K.; Lin, Y.-C.; Dai, C.-A.; Tseng, F.-G.; Pan, C.-Y.; Chen, Y.-T. Detection of K+ efflux from stimulated cortical neurons by an aptamer-modified silicon nanowire field-effect transistor. *ACS Sens.* **2017**, *2*, 69−79.

(28) Yoshida, K.; Mukai, Y.; Niidome, T.; Takashi, C.; Tokunaga, Y.; Hatakeyama, T.; Aoyagi, H. Interaction of pleurocidin and its analogs with phospholipid membrane and their antibacterial activity. *J. Pept. Res.* **2001**, *57*, 119−126.

(29) Lan, Y.; Ye, Y.; Kozlowska, J.; Lam, J. K. W.; Drake, A. F.; Mason, A. J. Structural Contributions to the Intracellular Targeting Strategies of Antimicrobial Peptides. *Biochim. Biophys. Acta, Biomembr.* **2010**, *1798*, 1934−1943.

(30) Mason, A. J.; Chotimah, I. N. H.; Bertani, P.; Bechinger, B. A. Spectroscopic Study of the Membrane Interaction of the Antimicrobial Peptide Pleurocidin. *Mol. Membr. Biol.* **2006**, *23*, 185−194.

(31) Syvitski, R. T.; Burton, I.; Mattatall, N. R.; Douglas, S. E.; Jakeman, D. L. Structural Characterization of the Antimicrobial Peptide Pleurocidin from Winter Flounder. *Biochemistry* **2005**, *44*, 7282−7293.

(32) Saint, N.; Cadiou, H.; Bessin, Y.; Molle, G. Antibacterial Peptide Pleurocidin Forms Ion Channels in Planar Lipid Bilayers. *Biochim. Biophys. Acta, Biomembr.* **2002**, *1564*, 359−364.

(33) Beseničar, M.; Maček, P.; Lakey, J. H.; Anderluh, G. Surface plasmon resonance in protein-membrane interactions. *Chem. Phys. Lipids* **2006**, *141*, 169−178.

(34) Cooper, M. A.; Hansson, A.; Löfås, S.; Williams, D. H. A vesicle capture sensor chip for kinetic analysis of interactions with membrane-bound receptors. *Anal. Biochem.* **2000**, *277*, 196−205.

The study of HIV-1 Vpr-membrane and Vpr-hVDAC-1 interactions by Graphene Field-Effect Transistor Biosensors

Peibin Zhong,[‡] Chun-Hao Liu,[§#] Yit-Tsong Chen,*[‡†] and Tsyr-Yan Yu*[†]

[‡]Department of Chemistry, National Taiwan University, 1, Sec. 4, Roosevelt Rd., Taipei 10617, Taipei, Taiwan

[†]Institute of Atomic and Molecular Sciences, Academia Sinica, 1, Sec. 4, Roosevelt Rd., Taipei 10617, Taiwan

[§]Chemical Biology and Molecular Biophysics, Taiwan International Graduate Program, Academia Sinica, Taipei, 115, Taiwan

[§]Institute of Bioinformatics and Structural Biology, National Tsing Hua University, Hsin Chu, Taiwan 30013, ROC.

Corresponding Authors
Yit-Tsong Chen
Department of Chemistry, National Taiwan University, 1, Sec. 4, Roosevelt Rd., Taipei 10617, Taipei, Taiwan; Phone: +886 (2) 3366-8198; Email: ytcchem@ntu.edu.tw

Tsyr-Yan Yu
Institute of Atomic and Molecular Sciences, Academia Sinica, 1, Sec. 4, Roosevelt Rd., Taipei 10617, Taiwan; Phone: +886 (2) 2366-8210; Email: tyyu@pub.iams.sinica.edu.tw

Peibin Zhong and Chun-Hao Liu have contributed equally to this work.

1. Expression, purification, and characterization of viral protein R

The original *vpr* gene sequence of human immunodeficiency virus type 1 *(HIV-1) group M subtype B* was obtained from the National Center for Biotechnology Information (NCBI) search database, with the NCBI reference protein sequence NP_057852.2 and UniProtKB/Swiss-Prot P69726. The *vpr* gene sequence was codon-optimized for *E. coli* expression and synthesized by Genomics BioSci & Tech (New Taipei City). The DNA sequence of the synthetic *vpr* gene is listed below.

ATGGAACAGGCACCGGAAGATCAGGGTCCGCAGCGTGAACCGCATA ATGAATGGACCCTGGAACTGCTGGAAGAACTGAAAAATGAAGCAGTTCGT CATTTTCCGCGTATTTGGCTGCATGGTCTGGGTCAGCATATTTATGAAACC TATGGTGATACCTGGGCAGGCGTTGAAGCAATTATTCGTATTCTGCAGCA ACTGCTGTTTATCCATTTTCGTATTGGTTGTCGTCATAGCCGTATTGGTGTT ACCCGTCAGCGTCGTGCACGTAATGGTGCAAGCCGTAGCTGA

The synthetic *vpr* gene was cloned by the restriction-free cloning method into the pET-15b expression vector, containing a 6x Histidine tag, followed by a GB1 tag, and the cleavage site of tobacco etch virus (TEV) protease, at the N-terminal. The final expression vector carried 6xHis-GB1-TEV-Vpr, hereinafter referred to as GB1-fused Vpr as illustrated in Fig. 1(A). The Vpr proteins were expressed in the *E. Coli* BL21 (DE3) strain. An overnight culture in LB broth, supplemented with carbenicillin at the concentration of 100 μg/mL, was prepared at 37°C. Cells were then sub-cultured in LB broth or a defined growth medium[S1] at 20°C (Table S1), and the overexpression of GB1-fused Vpr protein was induced by the addition of 0.1 mM IPTG when the cell density reached $OD_{600\ nm} = 0.7\text{-}0.9$. An extra amino-acid mixture, including 50 mg of each of the 20 amino acids, was added after induction, and the culture was grown at 18°C for 24 hr for protein expression. The bacterial cells were harvested by centrifugation for 15 min at 6,000 rpm, using an Avanti J-26S XP centrifuge operated with a JLA 8.1000 rotor at 4°C. For GB1-fused Vpr purification, the cell pellet was re-suspended in lysis buffer (50 mM Tris at pH 8.0, 250 mM NaCl, 5 mM β-mercaptoethanol, 1 tablet Roche cOmplete™ Mini EDTA-free tablet, 5 mM MgCl₂, 2 mg DNase Ⅰ and 2 mg lysozyme) and disrupted using a sonicator (Q700, Qsonica, Newtown, CT). A sucrose cushion centrifugation (50 mM Tris at pH 8.0, 500 mM NaCl, 50% w/w sucrose), performed for 45 min at 15,000 rpm (JA 25.50 rotor, Beckman

Coulter, Irving, TX), was used to collect the insoluble components containing GB1-fused Vpr protein. The supernatant was further centrifuged for 45 min at 15,000 rpm in lysis buffer to collect the insoluble part completely. Ni-NTA affinity chromatography was further used to purify the protein from the pellets in denaturing conditions at 4°C. The equilibration and binding buffer used for Ni-NTA affinity purification contained 50 mM Tris at pH 8.0, 100 mM NaCl, 5 mM imidazole, and 6 M guanidine hydrochloride (GdnHCl). After binding, the resin was sequentially washed with the binding buffer, wash buffer 1 (50 mM Tris at pH 8.0, 100 mM NaCl, 10 mM imidazole, and 6 M GdnHCl) and wash buffer 2 (50 mM Tris at pH 8.0, 100 mM NaCl, 20 mM imidazole, and 6 M GdnHCl) to remove impurities. The protein was eluted with the elution buffer (50 mM Tris at pH 8.0, 100 mM NaCl, 500 mM imidazole, and 6 M GdnHCl). Further dialysis against a buffer (25 mM Tris at pH 9.0, 100 mM NaCl, 1 mM EDTA, and 2 mM DTT) was performed twice to obtain GB1-fused Vpr proteins in both the soluble and insoluble forms. Further purification of the soluble GB1-fused Vpr proteins was performed by size-exclusion chromatography (SEC) using Superdex 200 Increase 10/300 (GE Healthcare, Chicago, IL) in a buffer containing 50 mM Tris at pH 9.0, 50 mM NaCl, 1 mM EDTA, and 0.5 mM Tris(2-carboxyehtyl)phosphine hydrochloride (TCEP). The analysis of high-resolution nanospray ESI mass spectrometry (LTQ FT Ultra, Thermo Scientific), documented in Table S3, revealed that the first methionine residues of the GB1-fused Vpr protein were absent.

2. Solubilization of Vpr in DPC detergent micelles and secondary structure characterization by circular dichroism spectroscopy

The Vpr protein precipitate was first dissolved in a denaturing buffer consisting of 50 mM sodium phosphate at pH 6.5, 50 mM NaCl, 0.5 mM TCEP, 1 mM EDTA, and 6 M GdnHCl, and then added in a dropwise manner to the refolding buffer, consisting of 50 mM sodium phosphate at pH 6.5, 50 mM NaCl, 0.5 mM TCEP, 1 mM EDTA, and 9 mM DPC. The process was carried out with a peristaltic pump (Masterflex® L/S®, IL) operating at a flow rate of 50 µl/min. The protein solution was further stirred overnight at 4°C and then dialyzed using a 6-8 kDa molecular weight cut-off (MWCO) dialysis membrane (Orange Scientific, Belgium) against a buffer containing 25 mM sodium phosphate at pH 7.5, 25 mM NaCl, 0.5 mM DTT, and 1 mM EDTA. The protein solution was concentrated using a 5 kDa MWCO Centricon

(Vivaspin Turbo 15, Sart, Goettingen, Germany) and purified by SEC using a Superdex 200 Increase 10/300 column in a buffer containing 25 mM sodium phosphate at pH 7.5, 25 mM NaCl, 1 mM EDTA, 0.5 mM TCEP, and 1.8 mM DPC. To study the secondary structure of Vpr in DPC detergent micelles, 5 μM Vpr solubilized with DPC buffer containing 25 mM sodium phosphate at pH 7.5, 25 mM NaCl, 1 mM EDTA, 1mM TCEP, and 4.6 mM DPC was prepared. The circular dichroism spectrum, with a bandwidth of 2 nm, at the scanning speed of 50 nm/min, step resolution of 0.2 nm and the data accumulations of 8 times across the spectral range of 180–300 nm, was recorded using Jasco CD spectrometer (J-815, Tokyo, Japan) with a 1-mm path length cell. The secondary structure content was analyzed by DichroWeb using CDSSTR program[S2] and SP175 as reference set which was optimized for 190-240 nm. The lowest data point used in the analysis was set to 190 nm, and the scaling factor was 0.95.

3. Preparation of Vpr in Bicelles

Vpr, solubilized in two kinds of q-0.1 bicelles, was prepared for the CD spectroscopic characterization, including bicelles made of DMPC/DPC mixture and DMPC:DMPG (50:50 w/w)/DPC mixture. The lipids were first dissolved in chloroform and then dried on the glass wall by nitrogen gas, followed with vacuum treatment for 1 hr to remove the residual organic solvent. The dried lipid film was resuspended in Vpr protein solution containing 25 mM sodium phosphate at pH 7.5, 25 mM NaCl, 6.4 mM DPC, 1 mM EDTA, and 1mM TCEP. After 10 x freeze-thaw cycles at 37°C and using liquid nitrogen, the bicelle was formed. The exact q value of the bicelles was further measured by 1D 1H NMR spectroscopy.
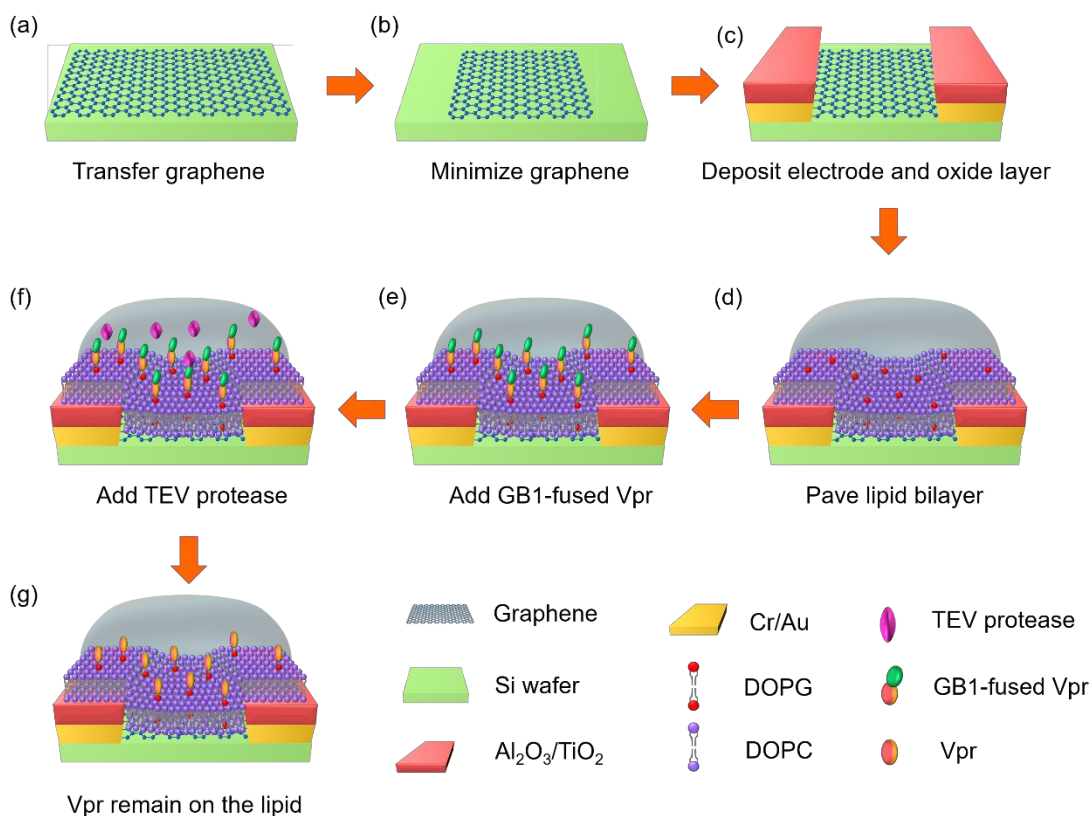
Figure S1. A schematic illustration of the fabrication of a SLB/G-FET device and the usage of this SLB/G-FET biosensor for detecting Vpr-membrane interactions. (a-b) A graphene film, transferred onto a Si wafer, was patterned by photolithography and casted by O_2 plasma to serve as the conducting channel (length:width = 2:1 μm) of a G-FET device. (c) A pair of source and drain electrodes (Cr/Au = 5/50 nm in thickness) was deposited with a thermal evaporation method. The Cr/Au electrodes were then coated with Al_2O_3/TiO_2 (60/5 nm in thickness) insulating layers by atomic-layer-deposition (ALD) to avoid electrical leakage in the following biosensing measurements. (d) After the fabrication of a G-FET device, a SLB was paved on top of the graphene channel (referred to as a SLB/G-FET), followed by embedding proteins into the SLB. (e) In the surface modification of SLB/G-FET, GB1-fused Vpr was first added on and inserted into a SLB/G-FET. (f) After 30 min of adding GB1-fused Vpr, TEV protease was injected to cut the GB1 off; (g) meanwhile, Vpr remained on the SLB.

(a) q=0.1, DPC/DMPC bicelles

(b) q=0.1, DPC/DMPC:DMPG bicelles
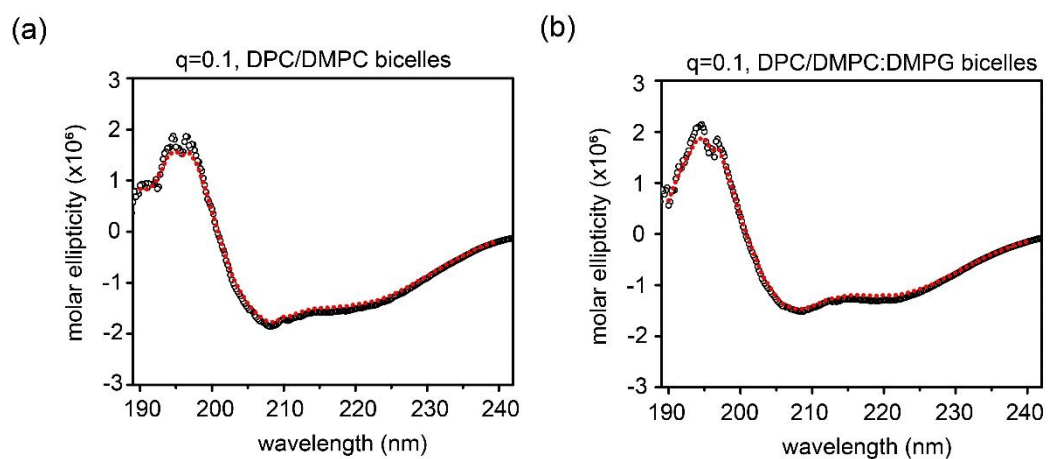
Figure S2. The CD spectra of Vpr solubilized in different membrane mimicking systems. The experimental (open circles) and fitted (dashed line) circular dichroism (CD) spectra of Vpr solubilized in (a) q=0.1 DPC/DMPC bicelles, (b) q=0.1 DPC/DMPC:DMPG (1:1) bicelles. The secondary structure content was analyzed by DichroWeb using a CDSSTR program and SP175 as a reference set which was optimized for 190-240 nm.
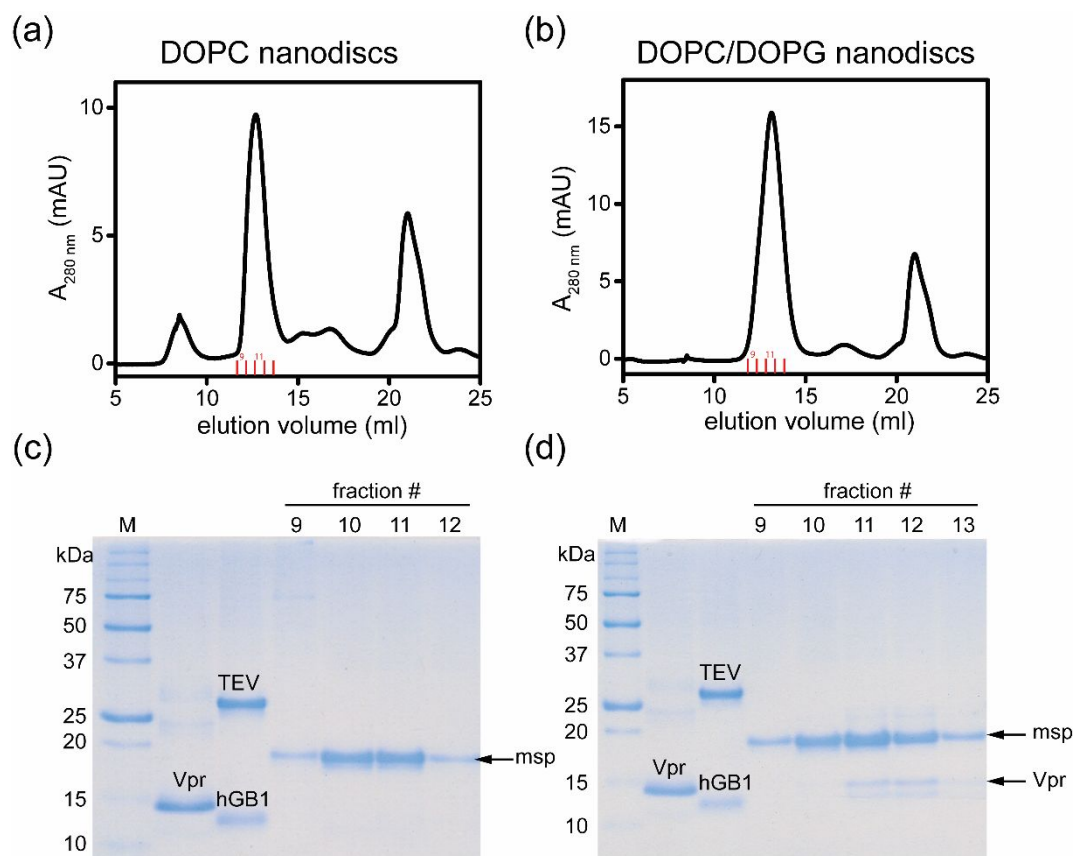
Figure S3. Lipid nanodisc co-assembly assay. The SEC profile of nanodiscs assembled with GB1-fused Vpr and DOPC lipids (a), and with GB1-fused Vpr and mixed DOPC/DOPG lipids in a 1:1 ratio (b). Each co-assembled nanodisc sample was treated with TEV protease prior to SEC analysis. The associated SEC fractions were analyzed by SDS-PAGE (c) and (d).
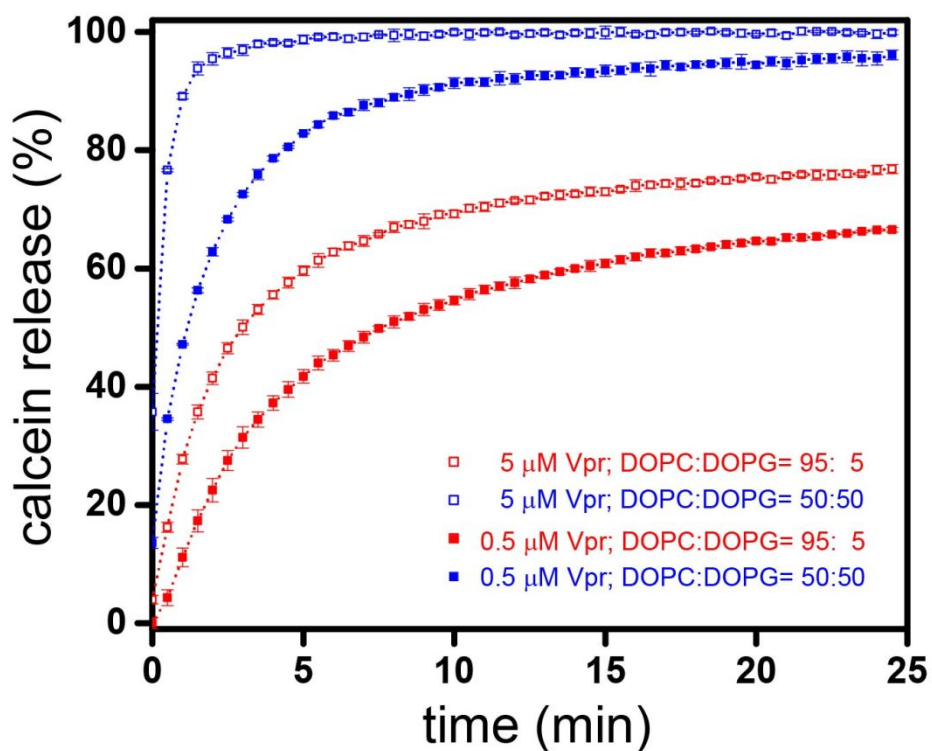
Figure S4. Protein concentration dependent permeabilization of liposomes by GB1-fused Vpr. Kinetics of calcein leakage of liposomes induced by GB1-fused Vpr at the concentrations of 0.5 and 5 μM, respectively. The extent of calcein release was quantified relative to a positive control (100%) sample that was solubilized with Triton X-100 detergent micelles, and a negative control (0%) sample with buffer only. The values are averages of triplicate assays in three experiments, with error bars representing standard deviation.
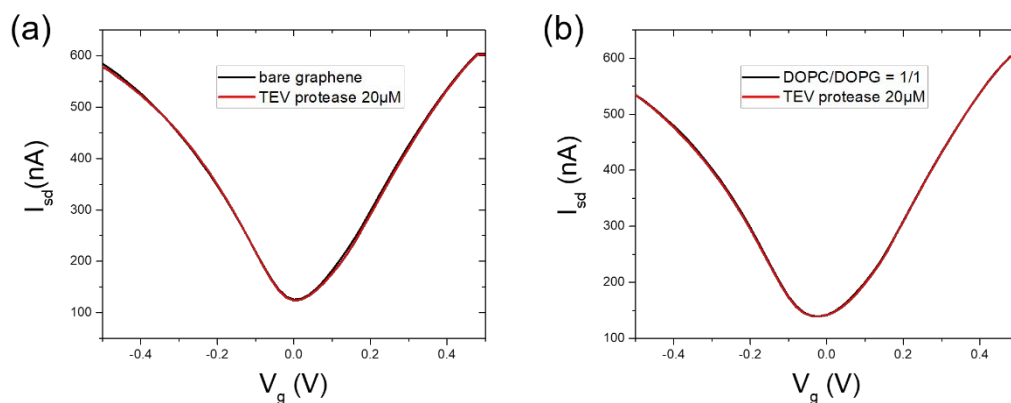
Figure S5. Validation experiments for examining the potential interaction between TEV and the biosensors. No interaction was observed between TEV and (a) a bare G-FET or (b) a SLB/G-FET device, where the SLB contains a mixture of DOPC/DOPG = 1:1. In both tests, the transfer curves remained unmoved after adding TEV protease, indicating that TEV protease has no significant interaction with G-FET or the DOPC/DOPG lipid bilayer.
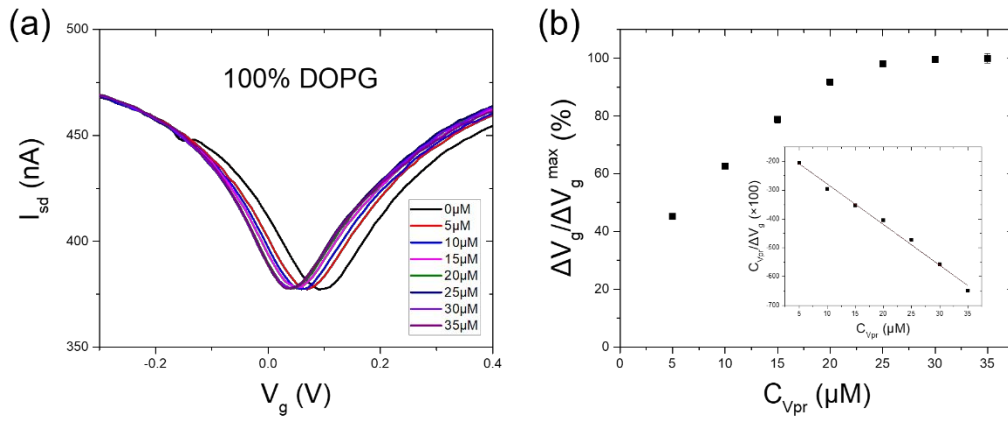
Figure S6. The response of a SLB/G-FET device to the addition of Vpr at C_{Vpr} = 0–35 µM, where the SLB was composed of pure DOPG. The left-shifts of the Dirac point of G-FET due to the additions of Vpr indicated the interaction of positively charged Vpr with the DOPG membrane to induce an n-doping in the G-FET. (b) The $\Delta V_g/\Delta V_g^{max}$ vs. C_{Vpr} plot is summarized from the data points measured in (a), where ΔV_g is the shift of the Dirac point relative to the buffer solution (without Vpr) and ΔV_g^{max} represents the saturated ΔV_g at high C_{Vpr}. The inset shows a least-squares fit of the measured data points to the Langmuir adsorption isotherm model, from which the dissociation constant of K_d = 7.3 ± 3.4 µM for the Vpr-DOPG complex was determined.
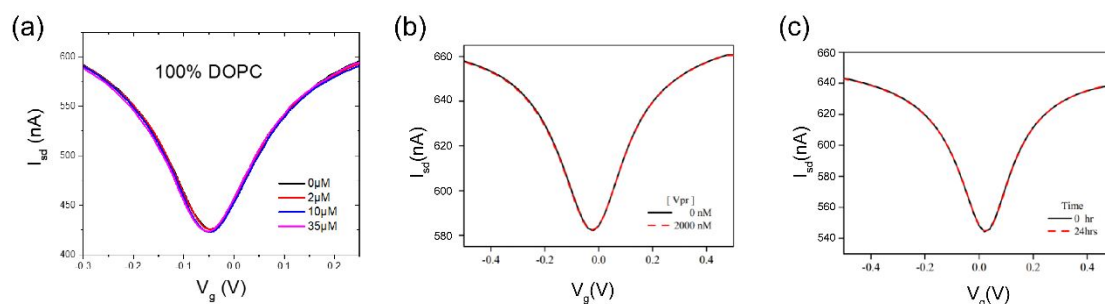
Figure S7. The control experiments for measuring the interaction of Vpr and hVDAC-1 embedded in DOPC membrane. (a) The response of a SLB/G-FET device was measured to the addition of Vpr, where the SLB was composed of DOPC lipids. The transfer curves were recorded as a function of C_{Vpr} from 0 to 35 μM. Only slight shift of the SLB/G-FET was detected with the addition of Vpr, indicating that the interaction between Vpr and the DOPC membrane was not significant. (b) The transfer curve of a G-FET device did not shift in response to the addition of Vpr, indicating that Vpr did not interact with a bare graphene. (c) The transfer curve of a G-FET device stayed unchanged for a period of 24 hrs, demonstrating the stability of the device.

Table S1. Recipe for 1L of growth medium. (Modified from reference [S1].)

1	1-liter salt solution	per liter
	K_2HPO_4	13.0 g
	KH_2PO_4	10.0 g
	Na_2HPO_4	9.0 g
	K_2SO_4	2.4 g
	NH_4Cl	1.0 g
2	100 µl Trace element solution	per 100 ml
	$MgCl_2 \cdot 6H_2O$	22.64 g
	HCl (12N)	0.16 ml
	$FeCl_2 \cdot 4H_2O$	400 mg
	$CaCl_2 \cdot 2H_2O$	15 mg
	H_3BO_3	6 mg
	$MnCl_2 \cdot 4H_2O$	1 mg
	$CoCl_2 \cdot 6H_2O$	2 mg
	$CuCl_2 \cdot 2H_2O$	1 mg
	$ZnCl_2$	28 mg
	$Na_2MoO_4 \cdot 2H_2O$	50 mg
3	100 µl Vitamin mixture solution	per liter
	Biotin (vitamin B7)	22 mg
	Folic acid (vitamin B9)	22 mg
	PABA (para-aminobenzoic acid)	2200 mg
	Riboflavin (vitamin B2)	2200 mg
	Pantothenic acid (vitamin B5)	4400 mg
	Pyridoxine HCl (vitamin B6)	4400 mg
	Thiamine HCl (vitamin B1)	4400 mg
	Niacinamide (vitamin B3)	4400 mg
4	Carbenicillin	100 mg
5	Glucose	4.0 g

Table S2. The yields of GB1-fused Vpr proteins.

	Soluble	Insoluble
Yield (mg/L LB broth)	3.6 ± 0.9	3.0 ± 0.7
Yield (mg/L defined growth medium)	10.1 ± 3.4	2.1 ± 0.5

Table S3. The monoisotopic mass (kDa) of the proteins.

Protein	Calculated mass	Observed mass
GB1-fused Vpr	21388.7	2138.6
Vpr	11315.8	11315.9

Table S4. Calculated Secondary Structure Fractions based on CD spectra.

	Helix 1	Helix 2	Strand 1	Strand 2	Turns	Unordered
DPC micelles	0.34	0.20	0.04	0.04	0.09	0.29
q=0.1 bicelles DPC/DMPC	0.37	0.21	0.03	0.03	0.13	0.23
q=0.1 bicelles DPC/DMPC: DMPG (1:1)	0.33	0.21	0.03	0.04	0.09	0.31

References

S1. Cai, M.; Huang, Y.; Sakaguchi, K.; Clore, G.M.; Gronenborn, A.M.; Craigie R. An efficient and cost-effective isotope labeling protocol for proteins expressed in shape Escherichia coli *J. Biomol. NMR* **1998**, *11*, 97–102.

S2. Sreerama, N.; Woody, R. W. Estimation of protein secondary structure from circular dichroism spectra: comparison of CONTIN, SELCON, and CDSSTR methods with an expanded reference set. *Anal. Biochem.* **2000,** *287* (2), 252–60.